Environ Geochem Health (2023) 45:665–686
https://doi.org/10.1007/s10653-022-01226-8

ORIGINAL PAPER

Check for updates

Radon and thoron concentrations in the southwest region of Angola: dose assessment and implications for risk mapping

Edson Baptista · Alcides J. S. C. Pereira · Filipa P. Domingos · Sérgio L. R. Sêco

Received: 28 August 2021 / Accepted: 13 February 2022 / Published online: 11 March 2022

Abstract Indoor radon (^{222}Rn) and thoron (^{220}Rn) are the most important natural sources of ionizing radiation to the public. Radiological studies that assess simultaneously ^{222}Rn and ^{220}Rn, and their controlling factors are particularly scarce in African countries. Hence, we conducted a survey of indoor ^{222}Rn and ^{220}Rn in buildings located in the SW region of Angola. Bedrock samples were also collected, and a borehole was executed to assess ^{226}Ra and ^{224}Ra activity concentration, ^{222}Rn and ^{220}Rn exhalation and emanation potential in the surface and at depth. The aim of this study was to determine the factors (geological and anthropogenic) that may influence the annual inhalation dose (AID) received by the population. Overall, the sum of indoor radon and indoor thoron concentrations, labelled the total indoor radon concentration (TIRC), was higher than 300 Bq/m^3 in only 5% of the buildings studied. The contribution of ^{220}Rn to the TIRC averaged 35% but may reach 95%, demonstrating the relevance of discriminating radon and thoron in indoor radon surveys. Indoor ^{222}Rn and ^{220}Rn were not correlated, indicating both must be estimated to properly assess the AID. Indoor ^{220}Rn concentrations were statistically different according to the building materials and type of usage. Higher ^{222}Rn and ^{220}Rn concentrations were observed in dwellings compared to workplaces. The median AID estimated for dwellings was 1.50 mSv/y compared to 0.26 mSv/y for workplaces, which are lower than the estimated average radiation exposure due to natural sources of 2.4 mSv/y. AID values higher than 1 mSv/y effective dose threshold established in the Council Directive 2013/59/EURATOM for the purpose of radiation protection in workplaces were observed in 12% of the workplaces studied suggesting the need for mitigation measures in those buildings. The analysis of bedrock samples revealed statistically significant correlations between ^{224} and ^{226}Ra activity concentration, and ^{220}Rn and ^{222}Rn exhalation and emanation potential. The borehole samples indicated a strong influence of weathering processes in the distribution of radioisotopes. The highest ^{226}Ra and ^{224}Ra activity concentration, and ^{222}Rn and ^{220}Rn exhaled per unit mass, TIRC and AID were observed in association with A-type

Supplementary Information The online version contains supplementary material available at https://doi.org/10.1007/s10653-022-01226-8.

E. Baptista · A. J. S. C. Pereira · F. P. Domingos · S. L. R. Sêco (✉)
Department of Earth Sciences, LRN – Laboratory of Natural Radioactivity, University of Coimbra, Pole II, Rua Sílvio Lima, 3030-790 Coimbra, Portugal
e-mail: osergioseco@gmail.com

A. J. S. C. Pereira
Department of Earth Sciences, CITEUC – Center for Earth and Space Research, University of Coimbra, Coimbra, Portugal

F. P. Domingos · S. L. R. Sêco
IATV – Instituto do Ambiente, Tecnologia e Vida, Coimbra, Portugal

red granites and porphyries. We conclude that both geological and anthropic factors, such as the type of building usage and building materials, must be considered in dose assessment studies and for the development of risk maps.

Keywords Radon · Thoron · Annual inhalation dose · Dwellings · Workplaces · Bedrock

Introduction

Indoor radon (^{222}Rn) and thoron (^{220}Rn) and their decay products represent the largest source of exposure to ionizing radiation in the population, causing lung cancer (WHO, 2009; UNSCEAR, 2010). ^{222}Rn and ^{220}Rn are noble gases formed in the radioactive decay series of uranium (^{238}U) and thorium (^{232}Th), respectively, and occur naturally in rocks and soils. Research efforts have been primarily focused on the study of ^{222}Rn concentration in dwellings, workplaces, building materials, water, caves, soil and bedrock units (e.g., Neznal et al., 1996; Åkerblom & Lindgren, 1997; Sainz et al., 2007; Appleton, 2013; A. Pereira, et al., 2013; Domingos & Pereira, 2018; Jorge & Pereira, 2020; Sêco et al., 2020; Domingos et al., 2021). The assessment of indoor ^{220}Rn concentrations has been underrated due to its short half-life and technical difficulties in its measurement, among other factors (e.g., Somogyi et al., 1984; Virk & Sharma, 2000; Tokonami, 2010; Vaupotic and Kávási, 2010). An increasing effort to discriminate and evaluate the concentration of both isotopes in dwellings has, however, been observed in the last few years (e.g., Kávási et al., 2007; Prasad et al., 2010; Mayya et al., 2012; Ramola et al., 2016; Zunic et al., 2017).

It is recognized that indoor ^{222}Rn and ^{220}Rn concentration are directly related to exhalation from bedrock, soil and the building materials (e.g., Kumar & Chauhan, 2014; Mann et al., 2015). Several lithological units such as granites, metamorphic rocks and sedimentary rocks present a distinctive radon exhalation potential, leading to an increased risk of exposure to ionizing radiation (e.g., Kemski et al., 2009; Scheib et al., 2013; A. Pereira et al., 2017; Sêco et al., 2020). The activity concentrations of ^{222}Rn and ^{220}Rn, and their progeny in dwellings are also influenced by anthropic factors and meteorological conditions, among others (see references above).

In the southernmost region of the African continent, ^{222}Rn and ^{220}Rn studies have been carried out mostly in Namibia, South Africa and Swaziland (e.g., Mahlobo & Farid, 1992; Nsibande et al., 1994; Farid, 1995; Mahlobo et al., 1995; Lindsay et al., 2008; Kgabi et al., 2009; Oyedele et al., 2010; Njinga et al., 2016; Botha et al., 2017; Munyaradzi et al., 2018). In Angola, studies on this subject are limited to the determination of ^{222}Rn and ^{220}Rn in 45 dwellings along with the concentration of radioelements in building materials (adobe) in Cabinda, Huambo and Menongue (Salupeto-Dembo et al., 2018, 2020). Measurements of ^{222}Rn were also conducted in 75 dwellings located in Lubango (Bahu et al., 2021). The relationship between the geological and anthropic factors, and indoor radon and thoron concentrations is still far away from being understood, not only in Angola but in the African continent. Beyond this, few studies have reported the results of simultaneous measurements of indoor radon and thoron concentrations in the literature in other regions of the world.

The Angolan territory is vast and composed of several geological units which may present highly variable concentrations of radionuclides. The national geological database of Angola has been recently updated, being subjected to several improvements (e.g., Carvalho et al., 2000; Delor et al., 2008; Pedreira & Waele, 2008; Batumike et al., 2009; Ferreira da Silva, 2009; E. Pereira et al., 2011, 2013a, 2013b; Lopes et al., 2016) which are crucial tools to the study of ^{222}Rn and ^{220}Rn distribution in the environment. The increase in knowledge on ^{222}Rn and ^{220}Rn distribution is critical to estimate the exhalation potential of geological materials that are commonly used as building materials in African countries, to model their spatial distribution and for the development of risk maps in the near future.

The main goal of this paper is to evaluate the distribution of ^{222}Rn and ^{220}Rn concentration and to identify the factors that may lead to an increased risk of exposure to these isotopes for the population. A survey of indoor ^{222}Rn and ^{220}Rn measurements in buildings of several counties located in the southwest region of Angola was carried out accounting for different types of bedrock units. To evaluate the role of the geological factors in the distribution of these gases, the concentration of their parent isotopes, namely ^{226}Ra and ^{224}Ra, and the emanation and exhalation power of ^{222}Rn and ^{220}Rn were determined in rock samples collected in outcrops and in a borehole. The anthropic factors were evaluated taken into account the building materials, the type of building usage and the habits of the inhabitants.

Of a broader significance, we demonstrate an effective link between the geological factors and indoor concentrations data and discuss the factors that may lead to higher indoor radon concentrations, posing a potentially significant health hazard due to an increased dose received by the population.

Geological framework

The Lubango, Quilemba, Humpata, and Matala counties are part of the Huila Plateau which is a part of the Angola portion of the Proterozoic Congo Craton (i.e., Angola-Kasai Block; e.g., Marques, 1977; Delor et al., 2008; Pedreira & Waele, 2008; Batumike et al., 2009; Lopes et al., 2016). The region comprises a large variety of lithological units that have been thoroughly studied (e.g., Torquato et al., 1979; Matias, 1980; Carvalho, 1983, 1984; Carvalho & Alves, 1993; Carvalho et al., 2000; Ferreira da Silva, 2009; E. Pereira et al., 2011, 2013a, 2013b; Lopes et al., 2016; and references therein). E. Pereira et al. (2013b) presented a simplified classification for the units studied in the present work that include the: (1) Pre-Eburnean basement (PEB); (2) Eburnean episode units; (3) Post-Eburnean rocks; and (4) Kibarean distension units which are described summarily in Fig. 1.

Material and methods

The detectors for the measurement of indoor ^{222}Rn and ^{220}Rn concentration and bedrock samples were prepared and analyzed at Laboratory of Natural Radioactivity of the Department of Earth Sciences of University of Coimbra (LRN-UC), which complies with the accreditation criteria for testing laboratories established in ISO/IEC 17,025:2017 for the measurement of indoor radon using passive detectors according to ISO 11665-4 and the activity concentration of ^{226}Ra, ^{232}Th and ^{40}K in construction natural and man-made materials, including soils and bedrock samples according to ISO 18589-3.

Indoor radon and thoron

About 98 passive detectors of the RADUET type (from Radosys Ltd.) were used for the measurement of indoor ^{222}Rn and ^{220}Rn concentration in dwellings and workplaces through integration methods. RADUET detectors were developed and calibrated by the National Institute of Radiological Sciences (Zhuo et al. 2002; Tokonami et al., 2005; Sorimachi et al., 2012). They comprise two CR-39 discriminative polyallyl diglycol carbonate sensors (10×10 mm) with two selective chambers (denoted main and sensitive chambers) that record ^{222}Rn and ^{220}Rn tracks (see Tokonami et al., 2005). The performance of these detectors has been evaluated elsewhere (see Sorimachi et al., 2012), and they have been shown to provide similar results to other types of discriminative ^{222}Rn and ^{220}Rn passive and active detectors (see Zhuo et al. 2002; Szeiler et al., 2012; Omori et al., 2020).

Several factors were considered in the distribution of the 98 RADUET detectors for sampling of indoor ^{222}Rn and ^{220}Rn including: (1) the type of building usage (dwellings or workplaces); (2) the type of building materials (e.g., clay, concrete, metal, stone, filled or hollow bricks; see Fig. 2); and (3) the underlying bedrock materials (see Fig. 1).

About 81 detectors were placed at a height between 0.8 and 2.0 m from the ground in ground floor rooms with high occupancy factors. The detectors were placed in secure locations to prevent damages and away from heat and ventilation sources. The ventilation conditions were variable between the sampled buildings since the detectors were placed in dwellings and workplaces built with different construction materials and styles. Contrary to the recommendations stated in ISO 11665-4, the detectors were placed closely to the walls to attain a higher efficiency in thoron detection. The remaining detectors ($n=17$) were placed strategically in 6 distinct buildings to evaluate the influence of the proximity of the detectors to the floor and walls on indoor ^{222}Rn and ^{220}Rn results and thereby, the effectiveness of thoron detection.

The detectors were retrieved on average, after three months of exposure; however, some detectors were

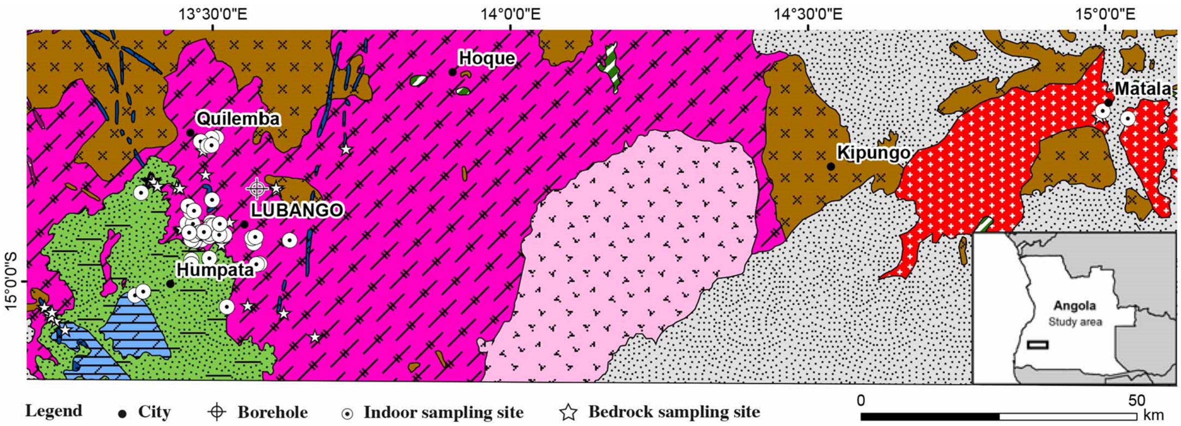

Geology			
Symbol	*Geological unit*	*Lithostratigraphy*	*References*
	Cenozoic cover	- Alluvial deposits, torrential and slope deposits;	E. Pereira et al. (2013b)
	Kibarean distension units	- Dolerites linked to deep fault systems with well defined orientations; - A-type red granites and porphyritic rhyolites occurring along NE-SW fault systems; - Anorthosite Complex - Post-Eburnean mafic rocks (PEMR) [Post-Eburnean mafic rocks (PEMR) and Anorthosite Complex formed by underplate upper mantle melts affected by fractionation processes and crustal contamination]	E. Pereira et al. (2011); Torquato et al., (1979); Carvalho et al. (1987); Lopes et al. (2016).
	Post-Eburnean rocks	- Leba Formation (LF, dark dolomitic limestones with stromatolites); - Chela Group (CG): - Cangalongue Formation (interbedded argillite, limestone and arkosic sandstone layers); - Bruco Formation (CGB, volcanic and sandstone intercalations with conglomeratic levels); - Humpata Formation (CGH, volcanic and sandstone intercalations); - Tundavala Formation (CGT, intercalations of conglomerates, sandstones and pyroclastic materials).	Correia (1976); Torquato and Forgaça, (1981); Pedreira and Waele (2008) E. Pereira et al. (2011)
	Eburnean episode units	- Peraluminous leucocratic granites; - Metaluminous granites (e.g. Chela and Gandarengos granites); - Quartz-feldspathic porphyries; - Eburnean granitoids and migmatites (EGM); - Gabbro-dioritic Complex; - Eburnean metasedimentary units;	Matias (1980); E. Pereira et al. (2006, 2011, 2013a, 2013b); Lopes et al. (2016)
	Pre-Eburnean basement	- Gneiss-migmatite Complex with minor occurrences of granitoid rocks; - Schist-quartzite-amphibolite Complex with marble layers;	Carvalho and Alves (1993); Carvalho et al. (2000); E. Pereira et al. (2011, 2013a, 2013b)

Fig. 1 Simplified geological map of the study area displaying the location of indoor radon measurements, bedrock samples collected and the executed borehole. Adapted and reinterpreted from the third sheet of the Geological Map of Angola at the scale of 1: 1.000.000 (LNICT, 1980) and E. Pereira et al. (2013a, 2013b). The lithostratigraphical framework was retrieved from the published literature listed under references

exposed for periods of up to six months. The duration of sampling was adjusted between sampling sites to suit the assumed radioactivity as recommended in ISO 11665-4.

Following exposure, each detector was sealed and sent to LRN-UC. The detectors were then chemically revealed using the Radobath equipment (Radosys Ltd.), at a temperature and duration defined by the manufacturer. The tracks were counted with an automatic image analysis system, the Radometer 2000 Dosimetric Microscopy (Radosys Ltd.). Indoor ^{222}Rn and ^{220}Rn activity concentration were calculated according to ISO 11665-4. Background measurements from 10 non-exposed detectors were detracted from the total tracks count of the exposed detectors. Calibration factors were provided by the manufacturer

Fig. 2 Examples of building materials and styles: **A** Clay (Adobe); **B** Concrete block; **C** Metal (Metallic plates); **D** filled clay brick; **E** hollow clay brick; **F** Stone; **G** Adobe built housing; **H** Dwelling built with concrete blocks; **I** Construction with metal plates; and **J** Dwelling built with stones

(*Fc* in tracks/cm^2 per Bq.h/m^3). Data below the lower limit of detection (LLD) of 10 Bq/m^3 for indoor ^{222}Rn and 15 Bq/m^3 for indoor ^{220}Rn were replaced by 0.65 LLD after Palarea-Albaladejo and Martín-Fernandez (2013).

The study of the influence of the proximity of the detectors to the floor and walls on indoor ^{222}Rn and ^{220}Rn revealed a fivefold increase in the median indoor ^{220}Rn between detectors placed near the floor and/or walls (of 242 Bq/m^3), compared to detectors placed in a mid-ground level (49 Bq/m^3) (see Fig. 3). However, according to the results of the Mann–Whitney–Wilcoxon test, indoor ^{222}Rn ($W=33.0$, p value $=1.000$) and indoor ^{220}Rn ($W=47.5$, p value $=0.159$) were not

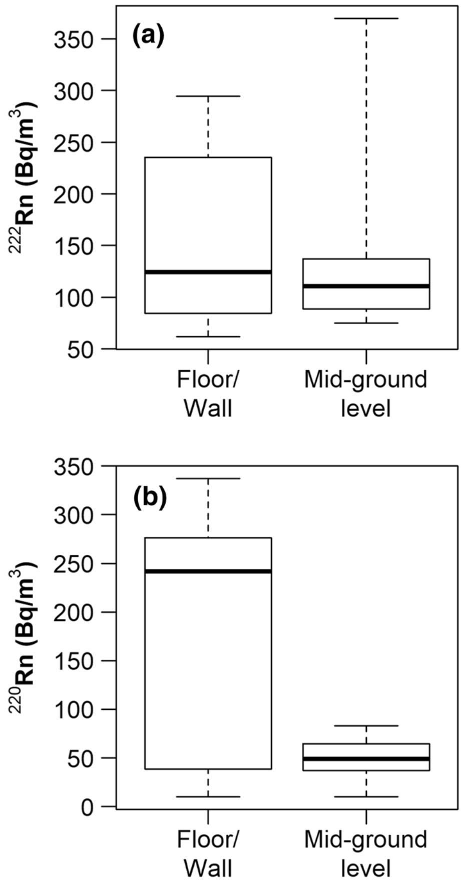

Fig. 3 Box and whiskers plots for comparison of **a** Indoor ^{222}Rn and **b** Indoor ^{220}Rn results from detectors placed closely to the floor and/or wall *versus* detectors placed in a mid-ground level

significantly different according to the detector placement strategy, which is probably due to a low sample size.

Bedrock samples

Fieldwork was carried out in the Lubango, Quilemba, Humpata and Matala counties. About 58 bedrock samples were collected for the determination of ^{226}Ra and ^{224}Ra activity concentration, ^{222}Rn and ^{220}Rn exhalation data and emanation coefficients, including 6 samples from a borehole. The samples were collected methodically according to the different types of rocks recognized in the study area, being considered representative of the geological unit sampled (Fig. 1). The selection of the sampling sites was supported by a preliminary assessment of the distribution of radionuclides (K, U and Th) in fresh and flat bedrock surfaces using a handheld gamma-ray (GR) spectrometer (RS-230, from Radiation Solutions) provided by LRN-UC following the procedure described in Sêco et al. (2021). Samples were collected taking into account the homogeneity of the GR spectrometer readings in order to improve the representativeness of the samples (Sêco et al., 2021). Areas covered by soil or vegetation were avoided, as well as uneven surfaces (e.g., Sêco et al., 2021).

The samples collected were dried in an oven at 70ºC, milled with a tungsten carbide mill and stored in radon proof *Marinelli* beakers. After at least 27 days, the samples were analyzed with a benchtop GR spectrometer from Ortec with a NaI (Tl) detector (3″ × 3″) mounted within a lead shield. The 1767.5 and 2614.5 keV isotopic lines were used to measure ^{214}Bi and ^{208}Tl, respectively. The measurements lasted 10 h and the spectra were analyzed with ScintiVision-32 (version 2, Ortec). Given that samples were stored until equilibrium between ^{222} and ^{220}Rn and their parent isotopes were attained, ^{214}Bi and ^{208}Tl activity are representative of ^{226}Ra and ^{224}Ra activity, respectively. The methodology is discussed in detail by Domingos and Pereira (2018). The estimated LLD for the sample set was 4.1 Bq/kg for ^{226}Ra and 1.7 Bq/kg for ^{224}Ra.

^{222}Rn and ^{220}Rn exhalation and emanation coefficients were determined with the accumulation method according to the procedure described in Domingos et al. (2021) using an AlphaGuard DF2000 monitor from Saphymo GmbH. The flow rate was set to 2 L/min, and the continuous Rn/Tn 2L measuring mode was used to discriminate between ^{222} and ^{220}Rn. According to Burkin and Villert (2017), the LLD for ^{222}Rn and ^{220}Rn when using the Rn/Tn 2L measuring mode when calculating the mean value of a 60 min period is 6 Bq/m^3 for ^{222}Rn and 12 Bq/m^3 for ^{220}Rn. The mean activity concentration of ^{222}Rn and ^{220}Rn was estimated by calculating the mean over a period of at least 1220 min (see also Domingos et al., 2021). The background ^{222}Rn concentration was monitored prior to each measurement and subtracted from the equilibrium concentration. The concentration of ^{222}Rn was corrected to correspond to the equilibrium concentration. The ^{222}Rn and ^{220}Rn exhaled per unit mass (EX) were determined with the following equation (Eq. 1):

$$EX = \frac{C \times V}{W} \tag{1}$$

where V is the free volume of the stainless-steel container, W is the weight of the sample (in kg), C is the equilibrium concentration of ^{222}Rn or ^{220}Rn (in Bq/m^3). The ^{222}Rn and ^{220}Rn emanation coefficients were estimated by dividing the ^{222}Rn and ^{220}Rn exhaled per unit mass by the activity concentration of ^{226}Ra or ^{224}Ra (in Bq/kg), respectively. Data below the LLD for ^{226}Ra, ^{224}Ra, ^{222}Rn and ^{220}Rn were replaced by 0.65 LLD (after Palarea-Albaladejo and Martín-Fernandez, 2013) prior to the computation of ^{222}Rn and ^{220}Rn exhalation and emanation coefficients.

To perform geochemical analyses by X-ray fluorescence (XRF), the samples were ultimately dried at 105 °C, grinded with an agate mill and sieved to a grain size lower than 125 µm. Fused beads were prepared by subjecting the samples to a maximum temperature of 1065 ºC in a Claisse LeNeo fusion instrument using a 1:10 sample to flux ratio composed by lithium metaborate and lithium tetraborate (in equal proportion) for measurement of major elements (see Domingos & Pereira, 2018). Pressed pellets were also prepared for the measurement of trace elements, namely U and Th concentrations. Analyses were performed at Instituto Pedro Nunes with an AXIOSmAX (PANalytical) spectrometer, calibrated with certified geological standards. Loss on ignition (LOI) was estimated through the weight loss after subjecting the samples to a temperature of 1065 °C in an oven.

Annual inhalation dose

The total annual inhalation dose (AID) (in mSv/y) due to inhalation of ^{222}Rn and ^{220}Rn and their progeny was estimated with the following equation (UNSCEAR, 2000):

$$\text{AID} = \left\{ \left(0.17 + 9 \times F_{\text{Rn}}\right) \times C_{\text{Rn}} + \left(0.11 + 40 \times F_{\text{Tn}}\right) \times C_{\text{Tn}} \right\} \times \text{OF} \times T \times 10^{-6} \tag{2}$$

where F_{Rn} and F_{Tn} are the equilibrium factors for ^{222}Rn and its progeny and ^{220}Rn and its progeny, respectively, which were assumed to be 0.4 for ^{222}Rn and 0.02 for ^{220}Rn (UNSCEAR, 2010); C_{Rn} and C_{Tn} are the measured ^{222}Rn and ^{220}Rn activity concentrations (in Bq/m^3); OF is the occupancy factor and T is the time of exposure. The values 0.17 and 9 correspond to dose conversion factors for ^{222}Rn and its progeny concentrations (in nSv), respectively, while the values 0.11 and 40 are the dose conversion factors for ^{220}Rn and its progeny concentrations (in nSv), which were retrieved from UNSCEAR (2000). The factor 10^{-6} allows the conversion of nSv into mSv.

The indoor occupancy factor was estimated from the time of exposure that was calculated as the difference between the number of hours in a year ($365 \times 24 = 8760$ h) and the time spent away from home, considered as the normal working period. According to the Angola Labor Law, the normal work period should not exceed 8 daily hours. Workers have the right to weekly days of rest, and the vacation period is 22 working days in each year. Angola has also 15 public holidays (source: https://en.wikipedia.org/wiki/Public_holidays_in_Angola, last accessed on December 7, 2021). Thus, working days were estimated to be 224, giving an estimated time spent away from home solely related to working of 1792 h, and an occupancy factor for workplaces around 0.20. Hence, the estimated time of exposure for indoor radon in dwellings was 6968 h, giving an occupancy factor of 0.79, which is similar to the indoor occupancy factor considered in UNSCEAR (2010) of 0.8.

Data analysis

Firstly, descriptive statistics, such as the mean, standard deviation, median, coefficient of variation, minimum and maximum, were estimated to summarize the data and to evaluate the dispersion. The distribution of the data was studied using the Shapiro–Wilk W test for normality and quantile plots. The Spearman Rank correlation coefficient was used to assess correlations. The influence of building materials, building usage and bedrock on ^{222}Rn and ^{220}Rn data was assessed through the Kruskal–Wallis test using those variables as categorical variables. Statistical significance was established at a level of 0.05. All statistical analyses were performed with R (R Core Team, 2021), using the packages *EnvStats* (Millard, 2013), *Hmisc* (Harrell, 2020), *psych* (Revelle, 2020) and *summarytools* (Contois, 2020).

Results and discussion

Indoor radon and thoron data

Descriptive statistics of ^{222}Rn and ^{220}Rn indoor measurements, the ratio between ^{222} and ^{220}Rn indoor concentrations and the total indoor radon concentrations (TIRC), which corresponds to the sum of ^{222}Rn and ^{220}Rn concentrations, are presented in Table 1.

The World Health Organization's (WHO) proposes a RL of 100 Bq/m^3 for indoor radon which may be extendable to 300 Bq/m^3 if the country-specific conditions inhibit attaining the RL mentioned above (WHO, 2009). Indoor ^{222}Rn data range from 7 to 227 Bq/m^3, being lower than 300 Bq/m^3 in all buildings studied. Indoor ^{220}Rn data range from 10 to 461 Bq/m^3, being higher than 300 Bq/m^3 in 3 out of 81 measurements (approximately 4% of the data). The TIRC is higher than 300 Bq/m^3 in 5% of the data. The mean and median indoor ^{222}Rn and ^{220}Rn are lower than 100 Bq/m^3 separately; however, the combined mean concentration of these isotopes is equal to 100 Bq/m^3 (see Table 1). Bahu et al. (2021) report indoor radon concentrations in Lubango similar to the TIRC measured in present work, ranging from 20 to 497 Bq/m^3 with a mean of 136 Bq/m^3 determined with standard CR-39 detectors, which do not allow for discrimination between ^{222} and ^{220}Rn.

Indoor ^{220}Rn data are more variable than ^{222}Rn indoor data as shown by the coefficient of variation (Table 1). The ratio between indoor ^{222}Rn and ^{220}Rn varies between 1:21 to 12:1, averaging 3:1. Hence, indoor ^{222}Rn concentrations can be considered generally higher than indoor ^{220}Rn concentrations. In fact, indoor ^{222}Rn concentrations are higher than indoor ^{220}Rn concentrations in 63 buildings (77% of the buildings studied). The proportion of ^{220}Rn in TIRC varies from 8 to 95%, averaging 35%.

^{222}Rn and ^{220}Rn indoor data present a positive asymmetry. ^{222}Rn distribution is platykurtic, whereas ^{220}Rn distribution is leptokurtic. The results of the Shapiro–Wilk W test indicate a significant deviation from normality (Table 1). The normal quantile plots for log-transformed data are presented as supplementary material. ^{222}Rn distribution is approximately log-normal, while ^{220}Rn data deviate from the log-normal distribution due to a considerable number of samples below the LLD (see Table 1). Thus, nonparametric

Table 1 Descriptive statistics of indoor ^{222}Rn and ^{220}Rn data

	^{222}Rn (Bq/m^3)	^{220}Rn (Bq/m^3)	TIRC[a] (Bq/m^3)	^{222}Rn/^{220}Rn
Number of samples	81	81	81	81
Mean	58	42	100	3
Standard deviation	47	78	94	3
Minimum	7	10	17	1/21
First quartile	26	10	44	1
Median	45	16	67	3
Third quartile	70	28	109	5
90th Percentile	106	77	217	8
Maximum	227	461	483	12
Median absolute deviation	33	9	40	3
Coefficient of variation (%)	82	185	93	85
Skewness	2	4	3	–
Kurtosis	4	14	6	–
Number of samples below the LLD	3 (4%)	39 (48%)	–	–
Number of samples equal to or above 300 Bq/m^3	0 (0%)	3 (4%)	4 (5%)	–
Number of samples equal to or above 100 Bq/m^3	10 (12%)	8 (10%)	24 (30%)	–
Shapiro Wilk W test (*p*-value)	<0.001*	<0.001*	<0.001*	–

*Significant at a 0.05 significance level

[a]Sum of indoor ^{222}Rn and indoor ^{220}Rn activity concentration

statistical methods were used to investigate the relationship between the studied variables. ^{222}Rn and ^{220}Rn indoor data are not correlated according to the results of the Spearman rank correlation coefficient ($R = 0.10$, $n = 81$, p value $= 0.377$), even if data below the LLD for ^{222}Rn and ^{220}Rn are excluded ($R = -0.05$, $n = 45$, p-value $= 0.745$).

Data were grouped by geological unit, building materials, and building usage in Fig. 4. The results of the Kruskal-Wallis test for indoor ^{222}Rn and ^{220}Rn data using geological units, building materials and usage as categorical variables are presented in Table 2.

Indoor ^{222}Rn and ^{220}Rn data are not significantly different between geological units (Table 2). Both are higher in A-type red granites and porphyritic rhyolites (RGP), showing median indoor ^{222}Rn and ^{220}Rn levels higher than WHO's RL of 100 Bq/m^3, and lower in Post-Eburnean Mafic Rocks (PEMR, Fig. 4). The RGP extend through intrusive bands with a NE-SW alignment, resulting from (probable) anorogenic (A-type) magmatism (Torquato et al., 1979; Carvalho et al., 1987; Drüppel et al., 2007). According to Drüppel et al. (2007), A-type granites from the felsic rock suite that intrudes the anorthosite rocks of the Kunene Intrusive Complex typically contain

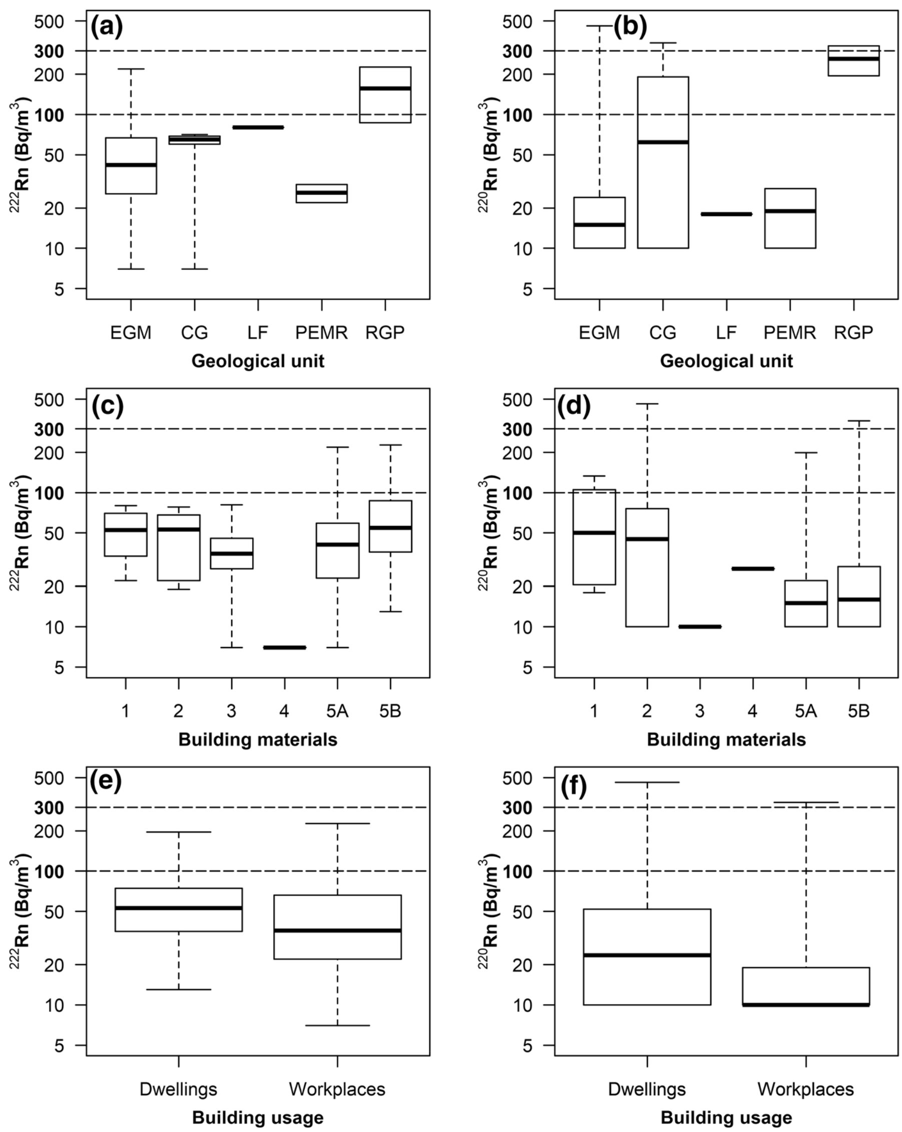

Fig. 4 Box and whiskers plots according to the geological units (**a**, **b**), construction materials (**c**, **d**) and building usage (e and f) for indoor ^{222}Rn (left) and indoor ^{220}Rn (right) concentrations. Geological units: EGM—Eburnean granitoids and migmatites; CG—Chela group; LF—Leba Formation; PEMR—Post-Eburnean Mafic Rocks; RGP—A-type red granites and porphyritic rhyolites. Building materials: 1—Clay; 2—Concrete; 3—Metal; 4—Stone; 5—Brick (5A—filled brick; 5B—hollow brick)

Table 2 Results of the Kruskal–Wallis test for indoor ^{222}Rn and ^{220}Rn data using geological units, building materials and usage as categorical variables (81 samples)

Variable of interest	Categorical variable	Chi-squared (χ^2)	*P*-value	Degrees of freedom
Indoor ^{222}Rn	Geological unit	7.320	0.120	4
	Building materials	7.193	0.207	5
	Building usage	2.446	0.118	1
Indoor ^{220}Rn	Geological unit	7.377	0.117	4
	Building materials	15.895	0.007*	5
	Building usage	9.711	0.002*	1

*Significant at a 0.05 significance level

abundant incompatible elements (Large Ion Lithophile and High Field Strength elements), including U and Th, which may justify the higher activity concentrations of ^{222}Rn and ^{220}Rn reported in this unit. The PEMR include dykes and sills of dolerites, gabbros and norites (LNICT, 1980). Low concentrations of U and Th are often observed in mafic rocks (e.g., Cinelli et al., 2019; Domingos et al., 2020), which may explain the lower indoor ^{222}Rn and ^{220}Rn activity concentrations observed in these units. The Chela Group (CG) presents higher median indoor ^{222}Rn and ^{220}Rn levels compared to the Eburnean granitoids and migmatites (EGM). The Leba Formation (LF) presents high median indoor ^{222}Rn levels, but comparatively low ^{220}Rn levels.

^{222}Rn data are not significantly different according to the building materials (Table 2), in contrast with indoor ^{220}Rn concentrations which are significantly different according to the building materials (Table 2). Clay and concrete-based building materials are associated with higher median ^{220}Rn levels, while lower ^{220}Rn levels are observed associated with metal and brick-based building materials (Fig. 4).

The influence of building usage was also assessed. Indoor ^{222}Rn are not significantly different between dwellings and workplaces, although higher median values are observed in dwellings (Table 2, Fig. 4). Indoor ^{220}Rn data are significantly different between dwellings and workplaces, with indoor ^{220}Rn levels being also higher in dwellings compared to workplaces (Table 2, Fig. 4).

Exhalation and emanation data

Descriptive statistics for ^{226}Ra and ^{224}Ra activity concentration, ^{222}Rn and ^{220}Rn exhaled per unit mass and their respective emanation coefficients are presented in Table 3. Samples retrieved from the borehole executed within a soil profile of an Eburnean granitoid were excluded from this analysis.

^{224}Ra activity concentration and ^{220}Rn exhaled per unit mass are higher on average than ^{226}Ra activity concentration and ^{222}Rn exhaled per unit mass, respectively, despite a similar range (Table 3). The median ^{222}Rn emanation coefficient is two times higher than the median ^{220}Rn emanation coefficient.

The distribution of ^{226}Ra, ^{224}Ra, ^{222}Rn and ^{220}Rn exhaled per unit mass and emanation coefficients are positively skewed. The distribution of ^{226}Ra is leptokurtic. The distribution of ^{222}Rn emanation is approximately mesokurtic, whereas the remaining variables present a platykurtic distribution. The results of the Shapiro–Wilk W test indicate a significant deviation from normality for all variables apart from the ^{220}Rn emanation coefficient (Table 3). The normal quantile plots for log-transformed data and the ^{220}Rn emanation coefficient are presented as supplementary material. The linearity observed in those plots indicates that the distribution of ^{226}Ra and ^{224}Ra activity concentration, ^{222}Rn and ^{220}Rn exhaled per unit mass and ^{222}Rn emanation coefficient is approximately log normal. Hence, nonparametric statistical methods were used to assess correlation between the variables (Table 4).

Statistically significant positive correlations are observed between all variables apart from ^{226}Ra activity concentration and ^{222}Rn emanation coefficient (Table 4). The correlation between ^{222} and ^{220}Rn exhaled per unit mass is stronger than the correlation between ^{222} and ^{220}Rn emanation coefficient, which is, in turn, stronger than the correlation between ^{226} and ^{224}Ra activity concentration. ^{226}Ra activity concentration and ^{222}Rn exhaled per unit mass, ^{224}Ra activity concentration and ^{220}Rn exhaled per unit mass also present strong correlations. The positive correlations observed indicate a good predictive power of ^{226}Ra

Table 3 Descriptive statistics of ^{226}Ra and ^{224}Ra activity concentration, ^{222}Rn and ^{220}Rn exhalation rate and emanation coefficients

	^{226}Ra (Bq/kg)	^{224}Ra (Bq/kg)	^{222}Rn exhaled per unit mass (Bq/kg)	^{220}Rn exhaled per unit mass (Bq/kg)	^{222}Rn emanation coefficient (%)	^{220}Rn emanation coefficient (%)
Number of samples	52	52	52	52	52	52
Mean	25.1	60.7	3.2	4.0	16	6
Standard deviation	24.2	39.3	3.2	3.4	12	3
Minimum	2.7	2.7	0.2	0.1	1	< 1
First quartile	7.1	35.1	0.9	1.5	7	4
Median	19.1	47.4	2.1	3.0	13	6
Third quartile	34.7	80.4	4.8	6.0	23	7
Maximum	133.4	169.5	11.8	14.9	56	13
Median absolute deviation	19.0	30.2	2.4	2.8	8	2
Coefficient of Variation (%)	96	65	98	86	77	45
Skewness	2.2	1.0	1.3	1.3	1.6	0.5
Kurtosis	7.0	0.4	0.7	1.5	3.1	0.1
Shapiro W test p value	< 0.001*	0.001*	< 0.001*	< 0.001*	< 0.001*	0.127

*Significant at a 0.05 significance level

Table 4 Spearman rank correlation matrix of radiological data

	^{226}Ra activity concentration	^{224}Ra activity concentration	^{222}Rn exhaled per unit mass	^{220}Rn exhaled per unit mass	^{222}Rn emanation coefficient	^{220}Rn emanation coefficient
^{226}Ra activity concentration	1.00					
^{224}Ra activity concentration	0.41*	1.00				
^{222}Rn exhaled per unit mass	0.68*	0.63*	1.00			
^{220}Rn exhaled per unit mass	0.46*	0.87*	0.78*	1.00		
^{222}Rn emanation coefficient	−0.22	0.41*	0.50*	0.57*	1.00	
^{220}Rn emanation coefficient	0.33*	0.43*	0.67*	0.79*	0.56*	1.00

*Significant at a significance level of 0.05

and ^{222}Rn data for estimating ^{224}Ra and ^{220}Rn in the study area.

Influence of surface weathering processes on exhalation and emanation data

The coefficient of variation observed in Table 3 indicates a lower variability of ^{224}Ra activity concentration compared to ^{226}Ra activity concentration, as well as a lower variability of ^{220}Rn exhaled per unit mass and emanation coefficients compared to ^{222}Rn values. These results contrast with observations made by Domingos et al. (2021) for granites sampled in the Central Iberian Zone (Portugal), where ^{224}Ra and ^{220}Rn were generally more variable than ^{226}Ra and ^{222}Rn, respectively. Given that this could indicate that the distribution of U and Th isotopes and their progeny in the study area might be constrained by differences in the relative mobility of these isotopes, further studies were conducted to determine the cause of the variability of the radiological variables studied.

The mobility of U is generally greater than Th in surface environments because U is soluble in the hexavalent state (U^{6+} or UO_2^{2+}; e.g., Boyle, 1982; Salminen et al., 2005; Regenspurt et al., 2010; Boekhout et al., 2015). Warm and humid paleoclimate conditions are associated with higher U mobility, due to leaching of U (e.g., Ruffell & Worden, 2000; Ruffell, 2016). These climate conditions are present in the Huila Plateau where four types of climates are recorded according to the Köppen–Geiger classification (e.g., Peell et al., 2007), namely: Cwb (Oceanic subtropical highland; West region), Cwa (subtropical humid; East region), Aw (tropical savanna; Northwest region) and BSh (warm semi-arid; South region). Thus, the higher variability of ^{226}Ra and ^{222}Rn may reflect the higher mobility of their parent isotope, suggesting a relevant control of surface weathering processes in the distribution of ^{226}Ra and ^{222}Rn in the study area. High $^{224}Ra/^{226}Ra$ ratios may also be connected to the climate conditions prevailing in the SW region of Angola (e.g., Burgess et al., 2004; Huntley, 2019).

To investigate the influence of surface weathering processes in the radiological properties of the bedrock, a borehole was executed in a soil profile with a thickness of 33 m developed over an Eburnean granitoid. About 6 samples were retrieved at specified depths in the borehole. The main results of the chemical and radiological analyses performed are shown in Fig. 5.

Loss on ignition (LOI) is a common proxy for chemical weathering due to its relationship with the volatile content (e.g., Gupta & Rao, 2001; Domingos & Pereira, 2018). LOI increases toward the surface, signposting a higher volatile content, which indicates a higher degree of chemical alteration toward the surface (Fig. 5).

^{224}Ra and ^{226}Ra activity concentration, Th and U concentration, ^{222}Rn and ^{220}Rn exhaled per unit mass and emanation coefficient increase until a 15 m depth and then, decrease in depth toward the slightly weathered bedrock sample retrieved at the end of the borehole. Similar trends were observed for the total iron (Fe_2O_3), magnesium (MgO) and titanium contents (TiO_2). These results indicate a concomitant accumulation of ^{224}Ra and ^{226}Ra with Fe_2O_3 and TiO_2 in ferralic horizons as a result of long and intensive weathering processes (e.g., Preetz et al., 2009). These horizons are typically associated with residual concentrations of kaolinite and highly resistant primary minerals (Preetz et al., 2009), which may justify the observed decrease in ^{222}Rn emanation coefficient, that is typically lower in highly resistant U-bearing minerals like zircon (e.g., Sakoda et al., 2011).

Along the soil profile, ^{226}Ra activity concentration ranges from 11.8 to 38.9 Bq/kg (with a coefficient of variation of 40%), showing a threefold increase at a depth of 15 m from the bedrock (base) level. ^{224}Ra is less variable (with a CV of 29%); nonetheless, a twofold increase is also observed at a 15 m depth. ^{222}Rn and ^{220}Rn exhaled per unit mass vary similarly (with a CV of 44 and 45%, respectively), being highest at

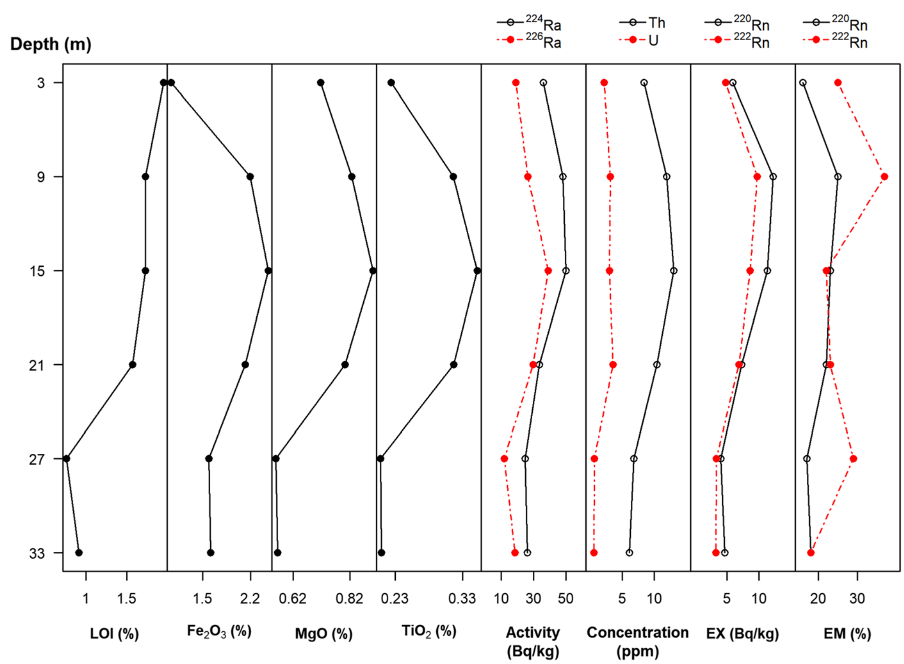

Fig. 5 Variation of chemical and radiological properties with depth (in m) through a borehole executed on a soil profile developed over an Eburnean granitoid. Results are shown for Loss on Ignition (LOI), total iron content (Fe_2O_3 in %), Magnesium (MgO, %), Titanium (TiO_2, %), ^{224}Ra and ^{226}Ra activity concentration, Th and U concentration (in ppm) measured by XRF, ^{222}Rn and ^{220}Rn exhaled per unit mass (EX in Bq/kg), and ^{222}Rn and ^{220}Rn emanation coefficients (EM in %)

a 9 m depth, where they present a threefold increase compared to the bedrock base level. The ^{222}Rn emanation coefficient is more variable than ^{220}Rn (CV of 26% compared to 18%), being lower in two scenarios: (1) closer to the surface (likely due to leaching of the parent isotopes which also show lower concentrations closer to surface), and (2) closer to the bedrock (associated with a lower degree of alteration indicated by LOI). The mobility of ^{226}Ra and ^{224}Ra with depth due to surface weathering processes and subsequent variation of the exhaled and emanated ^{222}Rn and ^{220}Rn corroborate the hypothesis of a strong influence of surface weathering processes in the distribution of these radioisotopes in the study area. Given the higher variability in depth of ^{226}Ra activity concentration and ^{222}Rn emanation coefficient compared to ^{224}Ra activity concentration and ^{220}Rn emanation coefficient, surface weathering processes may also justify the higher variability of the isotopes of this decay chain in the study area.

Influence of geological factors on exhalation and emanation data

Data were grouped by geological unit in Table 5 and Fig. 6. The Chela Group samples were divided according to the Formation sampled. The samples collected in outcrops of the Gandarengos granite were also separated from the remaining EGM samples. The results of the Kruskal–Wallis test are presented in Table 6. Apart from ^{226}Ra activity concentration and the ^{222}Rn emanation coefficient, all variables were

Table 5 Descriptive statistics by geological unit

Variable	Parameter	Geological unit								
		PEB	EGM	EGMG	CGT	CGH	CGB	LF	PEMR	RGP
Sample size	Number of samples	3	17	7	3	13	2	1	4	2
^{226}Ra (Bq/kg)	Median	11.1	20.4	43.0	17.2	7.2	6.3	4.5	13.3	44.6
	MAD	5.3	10.7	19.6	9.5	6.7	5.3	–	12.5	0.8
	CV	79	64	38	52	136	81	–	80	2
^{224}Ra (Bq/kg)	Median	80.2	44.7	98.2	51.7	47.1	22.1	8.1	19.5	145.7
	MAD	60.0	14.2	11.4	4.6	22.1	1.4	–	17.4	5.9
	CV	69	47	29	32	62	6	–	80	4
^{222}Rn exhaled per unit mass (Bq/kg)	Median	2.5	2.6	7.0	0.7	0.9	0.5	0.3	1.2	8.3
	MAD	0.7	1.2	2.1	0.4	0.4	0.1	–	0.7	4.7
	CV	89	73	29	48	162	16	–	94	55
^{220}Rn exhaled per unit mass (Bq/kg)	Median	4.7	2.7	7.2	1.1	2.4	1.0	0.2	1.1	13.0
	MAD	0.3	1.8	1.6	0.1	1.8	0.0	–	1.3	2.8
	CV	58	68	37	55	77	0	–	111	21
^{222}Rn emanation coefficient (%)	Median	27	13	16	4	9	9	7	11	19
	MAD	3	4	4	0	7	6	–	8	11
	CV	14	72	39	0	90	63	–	117	57
^{220}Rn emanation coefficient (%)	Median	7	6	9	4	5	5	3	5	9
	MAD	1	1	1	1	1	1	–	4	1
	CV	33	51	24	42	32	16	–	59	16
^{220}Rn ≥ ^{222}Rn exhaled per unit mass	Number of samples	3	10	4	3	10	2	0	1	2
	% of samples	100	59	57	100	77	100	0	25	100
^{220}Rn ≥ ^{222}Rn emanation coefficient	Number of samples	0	0	0	2	3	1	0	1	0
	% of samples	0	0	0	67	23	50	0	25	0

MAD, Median absolute deviation; CV, Coefficient of variation; PEB, Pre-Eburnean Basement; EGM, Eburnean granitoids and migmatites; EGMG, Eburnean granitoids and migmatites: Gandarengos granite; CGT, Chela Group, Tundavala Formation; CGH, Chela Group, Humpata Formation; CGB, Chela Group, Bruco Formation; LF, Leba Formation; PEMR, Post-Eburnean Mafic Rocks; RGP, A-type red granites and porphyritic rhyolites

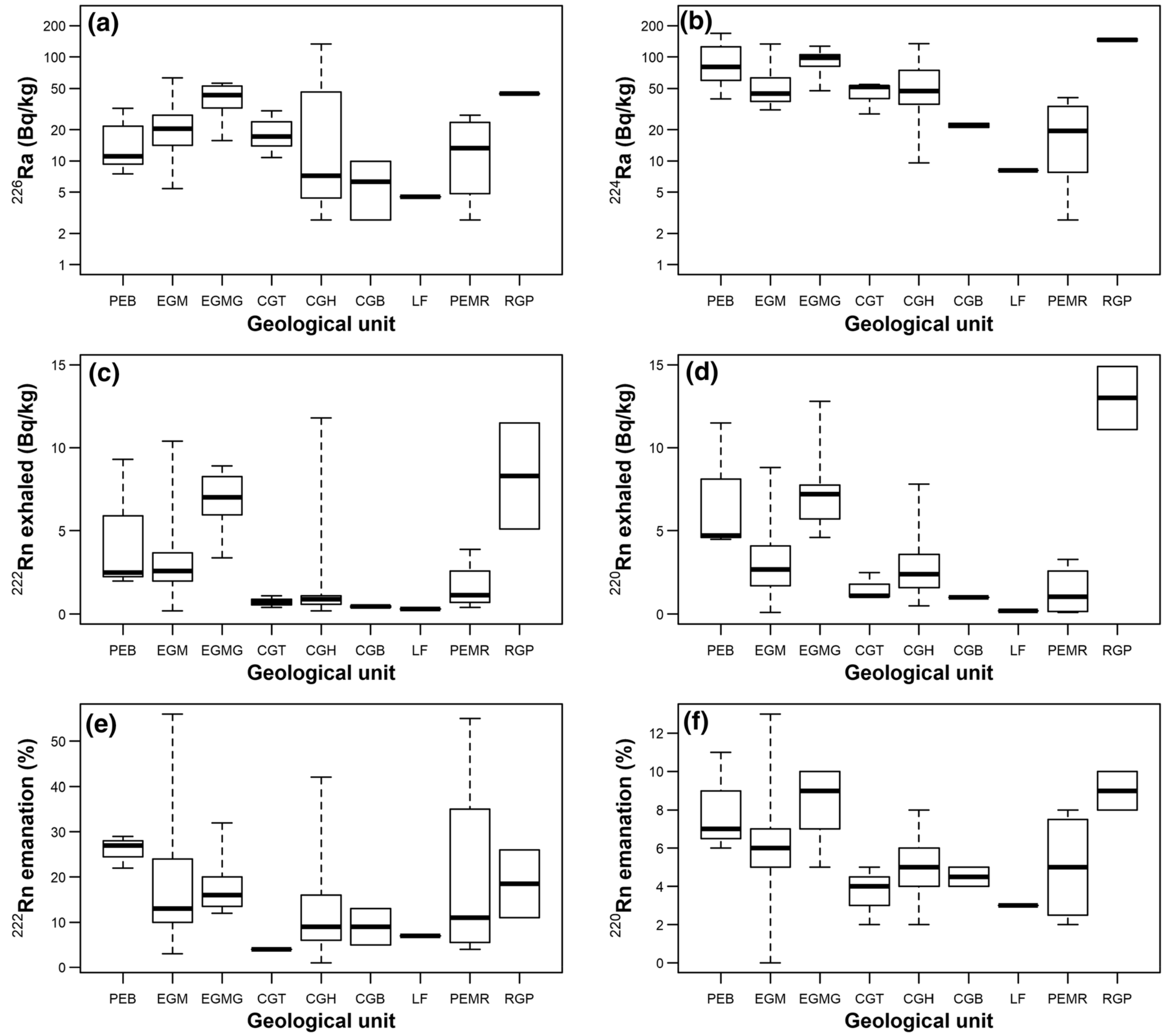

Fig. 6 Box and whiskers plots of **a** ^{226}Ra activity concentration; **b** ^{224}Ra activity concentration; **c** ^{222}Rn exhaled per unit mass; **d** ^{220}Rn exhaled per unit mass; **e** ^{222}Rn emanation coefficient; **f** ^{220}Rn emanation coefficient by geological unit. Geological units: PEB—Pre-Eburnean Basement; EGM—Eburnean granitoids and migmatites; EGMG—Eburnean granitoids and migmatites: Gandarengos granite; CGT—Chela Group, Tundavala Formation; CGH—Chela Group, Humpata Formation; CGB—Chela Group, Bruco Formation; LF—Leba Formation; PEMR—Post-Eburnean Mafic Rocks; RGP—A-type red granites and porphyritic rhyolites

Table 6 Results of the Kruskal–Wallis test for the radiological variables studied using geological units as categorical variable ($N=52$ samples)

Variable of interest	Chi-squared (χ^2)	*P* value	Degrees of freedom
^{226}Ra activity concentration	14.045	0.081	8
^{222}Rn exhaled per unit mass	28.398	<0.001*	8
^{222}Rn emanation coefficient	15.427	0.051	8
^{224}Ra activity concentration	24.539	0.002*	8
^{220}Rn exhaled per unit mass	26.254	0.001*	8
^{220}Rn emanation coefficient	18.109	0.020*	8

*Significant at a significance level of 0.05

statistically significantly different between geological units.

RGP presented the highest median ^{226}Ra and ^{224}Ra activity concentrations, ^{222}Rn and ^{220}Rn exhaled per unit mass, being followed by the Gandarengos granite (EGMG). The EGMG and RGP ^{226}Ra activity concentrations are similar to values reported by Pereira et al. (2017) in granites and orthogneisses associated with magmatic episodes that occurred before the Variscan orogeny close to relevant structural alignments (e.g., Ferreira et al., 1987), in an anorogenic context. The highest median ^{222}Rn emanation coefficients were, however, observed in the Pre-Eburnean Basement (PEB), followed by RGP, while the highest median ^{220}Rn emanation coefficients were observed in RGP, followed by EGMG.

The lowest median ^{226}Ra and ^{224}Ra activity concentration (4.5 Bq/kg and 8.1 Bq/kg, respectively), ^{222}Rn and ^{220}Rn exhaled per unit mass (0.3 Bq/kg and 0.2 Bq/kg, respectively) were observed in LF. The results for the LF are within the range of values reported by Sêco et al. (2020) in dolomitic limestones outcropping in the Lusitanian Basin (Portugal). The ^{222}Rn emanation coefficient with a median of 7% is also within the values reported by Sêco et al. (2020) for dolomitic limestones.

^{222}Rn and ^{220}Rn exhaled per unit mass were both higher in igneous and/or metamorphic basement (PEB, EGM, EGMG and RGP), and lower in sedimentary (CGT, CGH, CGB and LF) and mafic rocks (PEMR). The median ^{222}Rn emanation coefficient was lower than 20% in all geological units studied apart from PEB. The median ^{220}Rn emanation coefficient was lower than 10% in all geological units studied, averaging 6%. Higher median values for the ^{222}Rn and ^{220}Rn emanation coefficients were also observed in igneous and/or metamorphic units (PEB, EGM, EGMG and RGP), compared to sedimentary (CGT, CGH, CGB and LF) and mafic rocks (PEMR).

^{220}Rn exhaled per unit mass exceeded ^{222}Rn exhaled per unit mass in all samples collected in PEB, CGT, CGB and RGP (see Table 5). This is associated with $^{224}Ra/^{226}Ra$ ratios exceeding 3, and to a higher ^{220}Rn emanation coefficient in CGB. Over half of the samples from EGM, EGMG and CGH present ^{220}Rn exhalation values higher than ^{222}Rn. This indicates ^{220}Rn exhalation rate should not be disregarded in dose assessment studies, particularly if those materials are used as building materials.

Comparison of indoor and bedrock data

^{226}Ra and ^{222}Rn exhalation and emanation data of a building's underlying materials such as bedrock or soil have been widely used as predictors for indoor ^{222}Rn concentration (e.g., Singh et al., 2005; Gusain et al., 2009; Appleton et al., 2011; Bossew et al., 2013; Forkapic et al., 2017). The scatterplots of the median indoor ^{222}Rn and ^{220}Rn activity concentration by geological units against the median ^{226}Ra and ^{224}Ra activity concentration, ^{222}Rn and ^{220}Rn exhaled per unit mass and emanation coefficients are presented in Fig. 7. A linear relationship between indoor data and exhalation and emanation data appears to exist due to the particularly high median values observed for the RGP unit (Fig. 7). This suggests ^{226}Ra and ^{224}Ra activity concentration, and ^{222}Rn and ^{220}Rn exhalation and emanation could be useful for predicting indoor ^{222}Rn and ^{220}Rn activity concentration. However, further investigations are needed due to the low sample size ($n = 5$ geological units). Although the main source of indoor ^{220}Rn are the building materials, correlations between indoor ^{220}Rn and the soil content of ^{232}Th have been acknowledged in houses constructed with local soil materials (e.g., Shang et al., 2005). The relationship between indoor ^{220}Rn and bedrock ^{224}Ra activity concentration and ^{220}Rn exhaled per unit mass observed in Fig. 7 may be due to the fact that local raw materials are often used as building materials in the study area.

Assessment of the annual inhalation dose

The results of the estimated AID are presented in Table 7. The normal quantile plots for log-transformed data of the AID are presented as supplementary material. The linearity observed in the normal quantile plots for log-transformed AID data indicate that the distribution of AID for both dwellings and workplaces is approximately log-normal.

Table 7 shows the estimated AID for dwellings and workplaces, considering the occupancy factors presented in Sect. 3 of this paper. The AID was also estimated according to building material and the geological units using the occupancy factor estimated for dwellings to assess the influence of these parameters in the AID. The AID ranges from 0.51 to 5.28 mSv/y in dwellings (Table 7), with a median of 1.50 mSv/y, which is lower than the estimated

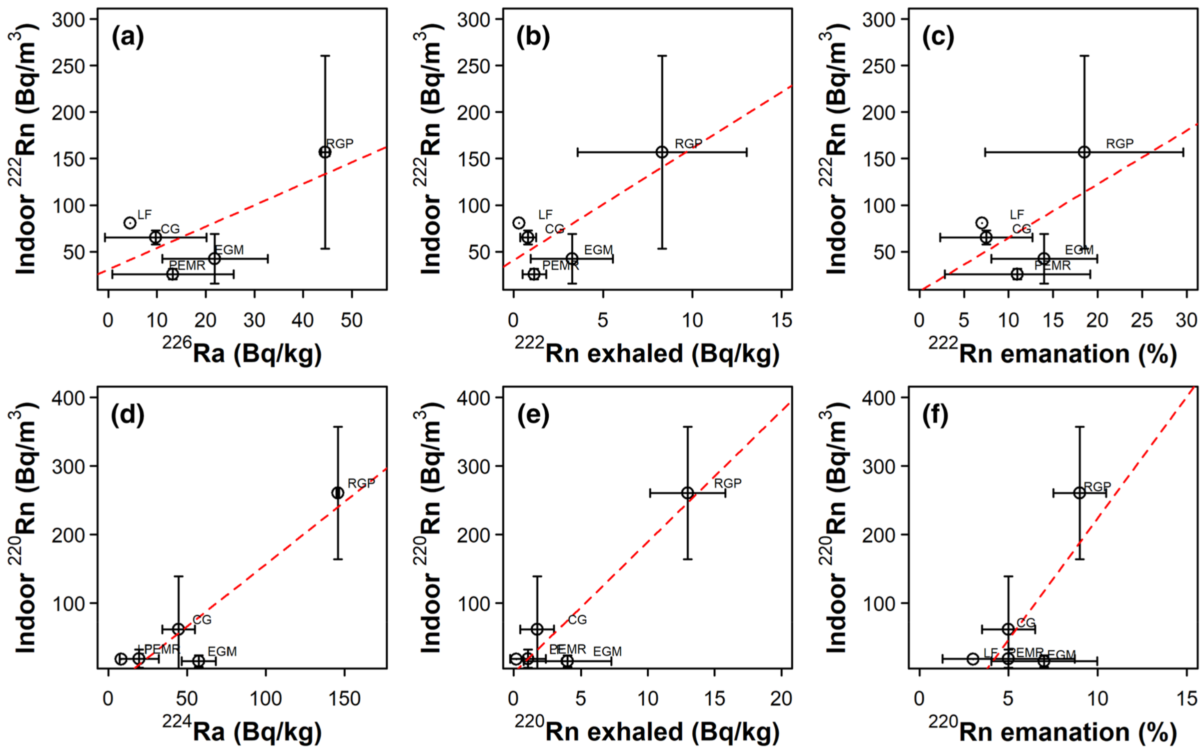

Fig. 7 Scatterplots of the median indoor ^{222}Rn activity concentration by geological units against the median **a** ^{226}Ra activity concentration; **b** ^{222}Rn exhaled per unit mass and **c** ^{222}Rn emanation coefficient and scatterplots of the median indoor ^{220}Rn activity concentration by geological units against the median: **d** ^{224}Ra activity concentration; **e** ^{220}Rn exhaled per unit mass; **f** ^{220}Rn emanation coefficient. The error bars correspond to the median absolute deviation. Legend: EGM—Eburnean granitoids and migmatites; CG—Chela Group; LF—Leba Formation; PEMR—Post-Eburnean Mafic Rocks; RGP—A-type red granites and porphyritic rhyolites

average radiation exposure due to natural sources of 2.4 mSv/y (UNSCEAR, 2010). The estimated mean value of the AID is similar to the values reported by Ramola et al. (2016) who conclude that the health risk due to exposure of radon, thoron and their progeny for that range of values is not significant.

Bahu et al. (2021) report AID values ranging from 2 to 7 mSv/y, with a global mean of 3.4 mSv/y for a similar time of exposure (7000 h). Differences in the mean AID between the results reported in the present work and Bahu et al. (2021) may be due to discrimination between ^{222} and ^{220}Rn carried out in the present work, given that ^{220}Rn may contribute up to 95% of the TIRC measured (see Sect. 4.1), corroborating the importance of discriminating between radon and thoron in dose assessment studies. In workplaces, given the lower occupancy factor, the AID ranges from 0.06 to 1.85 mSv/y, with a median of 0.26 mSv/y (Table 7).

Higher median AID values were observed in concrete-based constructions, followed by clay and brick constructions (Table 7). Lower AID median values were observed in metal and stone-based constructions. With respect to the geological units, higher median AID values were observed in the RGP unit, which was shown to present the highest median ^{226}Ra and ^{224}Ra activity concentrations, ^{222}Rn and ^{220}Rn exhaled per unit mass (see Fig. 6 and Table 5), beyond the highest median indoor ^{222}Rn and ^{220}Rn activity concentrations (Fig. 4). The lowest median AID was observed in the PEMR unit that also presented low values of ^{226}Ra and ^{224}Ra activity concentrations and ^{222}Rn and ^{220}Rn exhaled per unit mass compared to other geological units (Fig. 6 and Table 5). These results indicate that the characterization of the bedrock units is a useful proxy for dose assessment.

Table 7 Total annual inhalation dose (AID in mSv/y) due to inhalation of ^{222}Rn and ^{220}Rn and their progeny

	OF	N	AM	SD	Min	Q25	Med	Q75	Max	MAD	CV
Dwellings	0.79	40	1.89	1.02	0.51	1.20	1.50	2.44	5.28	1.06	54
Workplaces	0.20	41	0.44	0.42	0.06	0.19	0.26	0.46	1.85	0.15	95
Building materials											
Clay	0.79	4	1.76	0.66	1.07	1.27	1.78	2.27	2.42	0.81	38
Concrete	0.79	9	1.86	0.97	0.76	0.85	2.11	2.27	3.50	1.01	52
Metal	0.79	8	1.06	0.56	0.25	0.84	0.99	1.26	2.19	0.41	53
Stone	0.79	1	0.36	nd	nd	nd	nd	nd	nd	nd	nd
Filled brick	0.79	29	1.70	1.42	0.39	0.78	1.22	2.37	5.88	0.70	84
Hollow brick	0.79	30	2.11	1.58	0.46	1.07	1.50	2.69	7.20	1.02	75
Geological unit											
EGM	0.79	71	1.67	1.21	0.36	0.89	1.28	2.23	5.88	0.77	72
CG	0.79	5	2.21	1.39	0.25	1.77	2.21	2.79	4.05	0.86	63
LF	0.79	1	2.22	nd	nd	nd	nd	nd	nd	nd	nd
PEMR	0.79	2	0.80	0.06	0.76	0.78	0.81	0.83	0.85	0.07	8
RGP	0.79	2	5.78	2.02	4.35	5.06	5.78	6.49	7.20	2.11	35

OF, Occupancy factor; AM, Arithmetic mean; SD, Standard deviation; Min, Minimum; Q25, First quartile; Med, Median; Q75, Third Quartile; Max, Maximum; MAD, Median absolute deviation; CV, Coefficient of variation; EGM, Eburnean granitoids and migmatites; CG, Chela Group; LF, Leba Formation; PEMR, Post-Eburnean Mafic Rocks; RGP, A-type red granites and porphyritic rhyolites; nd, not determined

The empirical cumulative distribution function (ECDF) for dwellings and workplaces is presented in Fig. 8. The ECDF plot of the AID shows that the 1 mSv/y effective dose threshold established in the Council Directive 2013/59/EURATOM for the purpose of radiation protection in workplaces is exceeded in 12% of workplaces (5 out of 40). The workplaces where this threshold is exceeded are built over EGM ($n=3$) and the RGP ($n=2$) units, and the building materials used were filled ($n=2$) and hollow bricks ($n=3$).

Conclusions

This study presents ^{226}Ra and ^{224}Ra activity concentration, ^{222}Rn and ^{220}Rn exhalation in representative bedrock samples, an assessment of indoor ^{222}Rn and indoor ^{220}Rn activity concentrations measured in buildings and an estimation of the total AID due to inhalation of ^{222}Rn and ^{220}Rn and their progeny in both dwellings and workplaces located in the SW region of Angola. The major conclusions can be summarized as follows:

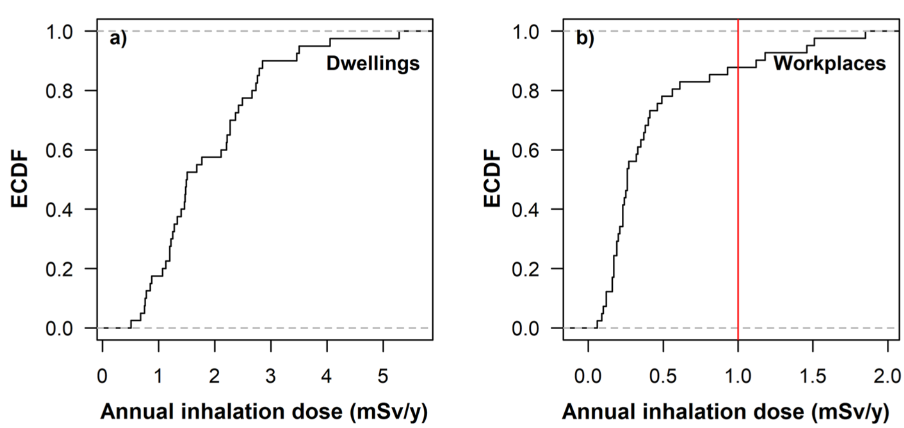

Fig. 8 Plots of the empirical cumulative distribution function (ECDF) of the annual inhalation dose (in mSv/y) for **a** dwellings and **b** workplaces

- Indoor radon levels are generally below 300 Bq/m^3;
- Indoor ^{222}Rn and indoor ^{220}Rn are not correlated indicating both must be estimated independently for a proper estimation of the contribution of ^{220}Rn to the AID;
- The contribution of ^{220}Rn to the TIRC averages 35% but may be dominating, reaching 95%;
- Indoor ^{222}Rn and indoor ^{220}Rn were not significantly different according to geological unit; however, indoor ^{220}Rn was significantly different depending on the building materials used as well as building usage;
- The AID has a median of 1.50 mSv/y in dwellings which is lower than the estimated average radiation exposure due to natural sources of 2.4 mSv/y (UNSCEAR, 2010), indicating that the health risks due to exposure of radon, thoron and their progeny in the study area are not significant according to Ramola et al. (2016);
- The highest indoor ^{222}Rn and ^{220}Rn activity concentrations were observed in buildings located above A-type red granites and porphyritic rhyolites;
- Clay and concrete-based building materials were associated with higher median ^{220}Rn levels and higher AID estimates, compared to metal and stone-based materials;
- Higher indoor ^{222}Rn and ^{220}Rn concentrations were observed in dwellings compared to workplaces.

The analysis of bedrock samples revealed that:

- ^{224}Ra activity concentration and ^{220}Rn exhaled per unit mass were higher but less variable than ^{226}Ra activity concentration and ^{222}Rn exhaled per unit mass, respectively;
- A significant variability of radiological properties with depth associated with surface weathering processes was observed;
- The highest ^{226}Ra and ^{224}Ra activity concentration, and ^{222}Rn and ^{220}Rn exhaled per unit mass were observed in A-type red granites and porphyritic rhyolites, similarly to indoor ^{222}Rn and ^{220}Rn indoor radon concentrations;
- Statistically significant correlations were observed between the radiological parameters studied.

The results of this study have several implications for the future development of risk maps in African countries, namely:

- Both indoor ^{222}Rn and indoor ^{220}Rn must be assessed independently to accurately determine the dose received by the population;
- The underlying bedrock materials, building usage and building materials should be considered in the design of sampling plans and the development of risk maps;
- Bedrock radiological data should be useful for estimating the risk of exposure to indoor ^{222}Rn and indoor ^{220}Rn.

Studies are still needed to assess the occupancy factors for a proper assessment of the AID based on the predominant lifestyle habits in the Angolan territory, that are significantly different from the lifestyle habits in developed countries. The estimation of the AID pertaining to workplaces is, however, expected to be accurate. If the 1 mSv/y effective dose threshold established in the Council Directive 2013/59/EURATOM is considered, then 12% of the workplaces studied where this threshold was exceeded would require mitigation measures.

Acknowledgements The authors acknowledge the financial and technical support provided by the Laboratory of Natural Radioactivity of the Department of Earth Sciences (University of Coimbra, Portugal), Instituto do Ambiente, Tecnologia e Vida (Portugal) and Instituto Pedro Nunes (Portugal). All participants in the indoor radon concentrations survey are also acknowledged.

Author's contributions Edson Baptista was responsible for sampling, sample preparation and drafting the article. Alcides J. S. C. Pereira was responsible for conception and design, sampling and for critically revising the article. Filipa P. Domingos was responsible for data analysis and interpretation, and drafting the article. Sérgio L. R. Sêco was responsible for data acquisition and drafting the article. All authors read and approved the final manuscript.

Declarations

Conflict of interest The authors have no relevant financial or non-financial interests to disclose. The authors are responsible for the correctness of the statements provided in the manuscript. The publication has been approved by all co-authors. All authors agree with the sequence of authors listed and the designated corresponding author. Data are available by request. Consent was obtained from all participants pertaining to the indoor radon measurements performed in the present work.

References

Åkerblom, G., & Lindgren, J. (1997). Mapping of groundwater radon potential. International Atomic Energy Agency, Vienna, 13–17 May, Vienna, Austria, (No. IAEA-TEC-DOC--980) (pp. 237–255).

Appleton, J. D. (2013). Radon in air and water. In O. Selinus et al. (Eds.), *Essentials of medical Geology: Revised Edition* (pp. 239–277). Dordrecht: Springer.

Appleton, J. D., Cave, M. R., Miles, J. C. H., & Sumerling, T. J. (2011). Soil radium, soil gas radon and indoor radon empirical relationships to assist in post-closure impact assessment related to near-surface radioactive waste disposal. *Journal of Environmental Radioactivity, 102*(3), 221–234.

Bahu, Y., Kessongo, J., Peralta, L., & Soares, S. (2021). Exposure to radon in buildings in the municipality of Lubango, Angola, during winter months. *Journal of Radioanalytical and Nuclear Chemistry, 327*(2), 635–642.

Batumike, J. M., Griffin, W. L., O'Reilly, S. Y., Belousova, E. A., & Pawlitschek, M. (2009). Crustal evolution in the central Congo-Kasai Craton, Luebo, DR Congo: Insights from zircon U-Pb ages, Hf-isotope and trace-element data. *Precambrian Research, 170*(1–2), 107–115.

Boekhout, F., Gérard, M., Kanzari, A., Michel, A., Déjeant, A., Galoisy, L., Calas, G., & Descostes, M. (2015). Uranium migration and retention during weathering of a granitic waste rock pile. *Applied Geochemistry, 58*, 123–135.

Bossew, P., Stojanovska, Z., Zunic, Z. S., & Ristova, M. (2013). Prediction of indoor radon risk from radium concentration in soil: Republic of Macedonia case study. *Romanian Journal of Physics, 58*(Suppl), 30–43.

Botha, R., Newman, R. T., Lindsay, R., & Maleka, P. P. (2017). Radon and thoron in-air occupational exposure study within selected wine cellars of the Western Cape (South Africa) and associated annual effective doses. *Health Physics, 112*(1), 98–107.

Boyle, R. W. (1982). *Geochemical prospecting for thorium and uranium deposits* (p. 498). Elsevier Scientific Publication Company.

Burgess, N., Hales, J. D., Underwood, E., Dinerstein, E., Olson, D., Itoua, I., Schipper, J., Ricketts, T., & Newman, K. (2004). *Terrestrial ecoregions of Africa and Madagascar: A conservation assessment* (p. 499). Island Press.

Burkin W., & Villert, J. (2017). Simultaneous Radon/Thoron discrimination using the AlphaGuard. Bertin Instruments, RADN-300-DE001, 22/02/2017.

Carvalho, H. (1984). Estratigrafia do Precâmbrico de Angola, 1ª aproximação. Centro de Geologia do Instituto de Investigação Científica Tropical. Garcia da Orta, Série Geologia, Lisboa, *7*(1-2), 1–66.

Carvalho, H., Crasto, J., Silva, Z., & Vialette, Y. (1987). The Kibaran Cycle in Angola: A discussion. In: Bowden, P., Kinnaird, J., (Eds.) *African Geology Reviews, Geological Journal*, *22*(1), 85–102.

Carvalho, H., & Alves, P. (1993). The Precambrian of SW Angola and NW Namíbia, general remarks, correlation analysis, economic geology, Comunicações do Instituto de Investigação Científica Tropical, Série de Ciências da Terra n. 4, Lisboa.

Carvalho, H. (1983). Notice explicative préliminaire sur la géologie de l'Angola. *Garcia De Orta. Série De Geologia, 6*(1–2), 15–30.

Carvalho, H., Tassinari, C., Alves, P. H., Guimarães, F., & Simões, M. C. (2000). Geochronological review of the Precambrian in western Angola: Links with Brazil. *Journal of African Earth Sciences, 31*(2), 383–402.

Cinelli, G., De Cort, M., & Tollefsen, T. (2019). *European atlas of natural radiation* (p. 190). Publication Office of the European Union.

Comtois, D. (2020). Summarytools: Tools to quickly and neatly summarize data. R package version 0.9.8. https://CRAN.R-project.org/package=summarytools

Correia, H. (1976). O Grupo da Chela e Formação da Leba como novas unidades litoestratigráficas resultantes da redefinição da Formação da Chela na região do Planalto da Humpata (Sudoeste de Angola). *Bol. Soc. Geol. Port., 20*, 65–130.

Delor, C., Theveniaut, H., Cage, M., Pato, D., Lafon, J.-M., Bialkowski, A., Rooig, J.-Y., Neto, A., Cavongo, M., & Sergeev, S. (2008). New insights into the Precambrian geology of Angola: Basis for an updated lithochronological framework at 1: 2000000 scale. In: *22nd Colloquium of African Geology, Hammame, Tunisia* (pp. 52–53).

Domingos, F., Cinelli, G., Neves, L., Pereira, A., Braga, R., Bossew, P., & Tollefsen, T. (2020). Validation of a database of mean uranium, thorium and potassium concentrations in rock samples of Portuguese geological units, generated of literature data. *Journal of Environmental Radioactivity, 222*, 106338.

Domingos, F., & Pereira, A. (2018). Implications of alteration processes on radon emanation, radon production rate and W-Sn exploration in the Panasqueira ore district. *Science of the Total Environment, 622*, 825–840.

Domingos, F. P., Sêco, S. L., & Pereira, A. J. (2021). Thoron and radon exhalation and emanation from granitic rocks outcropping in the Central Iberian Zone (Portugal). *Environmental Earth Sciences, 80*(22), 1–18.

Drüppel, K., Littmann, S., Romer, R. L., & Okrusch, M. (2007). Petrology and isotope geochemistry of the Mesoproterozoic anorthosite and related rocks of the Kunene Intrusive Complex, NW Namibia. *Precambrian Research, 156*(1–2), 1–31.

Farid, S. M. (1995). Passive track detectors for radon determination in the indoor environment. *Applied Radiation and Isotopes, 46*(2), 129–132.

Ferreira, N., Iglesias, M., Noronha, F., Pereira, E., Ribeiro, A., & Ribeiro, M. (1987). Granitoides da zona Centro-Ibérica e seu enquadramento geodinâmico. In: F., Bea, A., Gonzalo, Carnicero, J., Plaza, M., & Alonso, M. (Eds.), Geologia de los granitoides y rocas associados del Macizo Hesperico, libro homenage a L.C. Figueirola. Editorial Rueda, Madrid (pp. 37–51).

Ferreira da Silva, A. (2009). A geologia da República de Angola desde o Paleoarcaico ao Paleozóico Inferior. *Boetim De Minas, 44*, 99–162.

Forkapic, S., Maletić, D., Vasin, J., Bikit, K., Mrdja, D., Bikit, I., Udovičić, V., & Banjanac, R. (2017). Correlation analysis of the natural radionuclides in soil and indoor radon

in Vojvodina, Province of Serbia. *Journal of Environmental Radioactivity, 166*, 403–411.
Gupta, A. S., & Rao, S. K. (2001). Weathering indices and their applicability for crystalline rocks. *Bulletin of Engineering Geology and the Environment, 60*(3), 201–221. https://doi.org/10.1007/s100640100113
Gusain, G. S., Prasad, G., Prasad, Y., & Ramola, R. C. (2009). Comparison of indoor radon level with radon exhalation rate from soil in Garhwal Himalaya. *Radiation Measurements, 44*(9–10), 1032–1035.
Harrell, F. E. (2020). Hmisc: Harrell miscellaneous. R package version 4.4–2. https://CRAN.R-project.org/package=Hmisc
Huntley, B. J. (2019). Angola in outline: Physiography, climate and patterns of biodiversity. In B. J. Huntley, V. Russo, F. Lages, & N. Ferrand (Eds.), *Biodiversity of Angola* (pp. 15–42). Springer.
Jorge, M. P., & Pereira, A. J. S. C. (2020). A carsificação como fator potenciador de risco de radão: o caso das grutas da Moeda (Fátima–Portugal central) e região envolvente. *Comuunicações Geológicas, 107*(II), 173–177.
Kávási, N., Németh, C., Kovács, T., Tokonami, S., Jobbágy, V., Várhegyi, A., Gorjánácz, Z., Vígh, T., & Somlai, J. (2007). Radon and thoron parallel measurements in Hungary. *Radiation Protection Dosimetry, 123*(2), 250–253.
Kemski, J., Klingel, R., Siehl, A., & Valdivia-Manchego, M. (2009). From radon hazard to risk prediction-based on geological maps, soil gas and indoor measurements in Germany. *Environmental Geology, 56*(7), 1269–1279.
Kgabi, N. A., Mokgethi, S. A., & Bubu, A. (2009). Atmospheric radioactivity associated with gold mining activities in the North West Province of South Africa. *European Journal of Scientific Research, 33*(4), 594–605.
Kumar, A., & Chauhan, R. P. (2014). Measurement of indoor radon–thoron concentration and radon soil gas in some North Indian dwellings. *Journal of Geochemical Exploration, 143*, 155–162.
Lindsay, R., Newman, R. T., & Speelman, W. J. (2008). A study of airborne radon levels in Paarl houses (South Africa) and associated source terms, using electret ion chambers and gamma-ray spectrometry. *Applied Radiation and Isotopes, 66*(11), 1611–1614.
LNICT. (1980). Geologia de Angola, Carta na Escala 1/1000000, coordenada por Heitor de Carvalho, Laboratório Nacional de Investigação Científica Tropical, Folha n.º 3.
Lopes, F. C., Pereira, A. J., Mantas, V. M., & Mpengo, H. K. (2016). Morphostructural characterization of the western edge of the Huila Plateau (SW Angola), based on remote sensing techniques. *Journal of African Earth Sciences, 117*, 114–123.
Mahlobo, M., & Farid, S. M. (1992). Radon dosimetry using plastic nuclear track detector. *Journal of Islamic Academy of Sciences, 5*(3), 153–157.
Mahlobo, M., Nsibande, M., & Farid, S. M. (1995). Indoor ^{222}Rn measurements in Swaziland with the solid state nuclear track detector. *Journal of Environmental Radioactivity, 27*(3), 261–268.
Mann, N., Kumar, A., Kumar, S., & Chauhan, R. P. (2015). Radon–thoron measurements in air and soil from some districts of northern part of India. *Nuclear Technology and Radiation Protection, 30*(4), 294–300.
Marques, M. M. (1977). Esboço das unidades geomorfológicas de Angola (2ª aproximação). *Inst. Inv. Cient Trop. Garcia Orta, Serviços Geológicos, Lisboa., 2*, 41–43.
Matias, D. N. (1980). Carta Geológica de Angola à escala 1: 1000000 (folha 3). Instituto Geográfico Cadastral.
Mayya, Y. S., Mishra, R., Prajith, R., Gole, A. C., Sapra, B. K., Chougaonkar, M. P., Nair, R. R. K., Ramola, R. C., Karunakara, N., & Koya, P. K. M. (2012). Deposition-based passive monitors for assigning radon, thoron inhalation doses for epidemiological studies. *Radiation Protection Dosimetry, 152*(1–3), 18–24.
Millard, S. P. (2013). EnvStats: An R Package for Environmental Statistics. Springer. ISBN 978-1-4614-8455-4. https://www.springer.com
Munyaradzi, Z., Anna, K. N., & Makondelele, T. V. (2018). Excess lifetime cancer risk due to natural radioactivity in soils: Case of Karibib town in Namibia. *The African Review of Physics, 13*, 0012.
Neznal, M., Neznal, M., & Šmarda, J. (1996). Assessment of radon potential of soils—A five-year experience. *Environment International, 22*, 819–828.
Njinga, R. L., Tshivhase, M. V., Kgabi, N. A., & Zivuku, M. (2016). Hazards index analysis of Gamma emitting radionuclides in selected areas around the Uranium Mine sites at Erongo Region, Namibia. *Journal of Environmental Science and Management, 19*(2), 1–7.
Nsibande, M. C., Mahlobo, M., & Farid, S. M. (1994). Radon levels inside residences in Swaziland. *Science of the Total Environment, 151*(3), 181–185.
Omori, Y., Tamakuma, Y., Nugraha, E. D., Suzuki, T., Saputra, M. A., Hosoda, M., & Tokonami, S. (2020). Impact of wind speed on response of diffusion-type radon-thoron detectors to thoron. *International Journal of Environmental Research and Public Health, 17*(9), 3178.
Otoo, F., Darko, E. O., Garavaglia, M., Adukpo, O. K., Amoako, J. K., Tandoh, J. B., Inkoom, S., Nunoo, S., & Adu, S. (2021). Assessment of natural radioactivity and radon exhalation rate associated with rock properties used for construction in greater Accra region, Ghana. *Journal of Radioanalytical and Nuclear Chemistry*, 1–13.
Oyedele, J. A., Shimboyo, S., Sitoka, S., & Gaoseb, F. (2010). Assessment of natural radioactivity in the soils of Rössing Uranium Mine and its satellite town in western Namibia, southern Africa. *Nuclear Instruments and Methods in Physics Research Section a: Accelerators, Spectrometers, Detectors and Associated Equipment, 619*(1–3), 467–469.
Palarea-Albaladejo, J., & Martin-Fernandez, J. A. (2013). Values below detection limit in compositional chemical data. *Analytica Chimica Acta, 764*, 32–43.
Pedreira, A. J., & Waele, B. (2008). Contemporaneous evolution of the Palaeoproterozoic e mesoproterozoic sedimentary basins of the São Francisco-Congo Craton. *Geological Society, London, Special Publications, 294*, 33–48.
Peel, M. C., Finlayson, B. L., & McMahon, T. A. (2007). Updated world map of the Köppen-Geiger climate classification. *Hydrology and Earth System Sciences, 11*(5), 1633–1644.
Pereira, E., Van-Dúnem, M.V., & Tassinari, C.C.G. (2006). Carta Geológica de Angola, Notícia Explicativa da Folha

Sul D-33/N-III (Bibala), escala 1: 100 000:). Publicação do Instituto Geológico de Angola (p. 57).

Pereira, E., Rodrigues, J. F., Tassinari, C. C. G., Van-Dúnem, M. V. (2013a). Geologia da Região de Lubango, SW de Angola. Evolução no contexto do cratão do Congo. Instituto Geológico de Angola (p. 160).

Pereira, E., Rodrigues, J., Van-Dúnem, M. V. (2013b). Carta Geológica de Angola, à escala 1: 250 000: Folha Sul D-33/T (Chibia). Publicação do Instituto Geológico de Angola.

Pereira, A., Lamas, R., Miranda, M., Domingos, F., Neves, L., Ferreira, N., & Costa, L. (2017). Estimation of the radon production rate in granite rocks and evaluation of the implications for geogenic radon potential maps: A case study in Central Portugal. *Journal of Environmental Radioactivity, 166*, 270–277.

Pereira, A. J. S. C., Pereira, D., Neves, L., Peinado, M., & Armenteros, I. (2013). Radiological data on building stones from a Spanish region: Castilla y León. *Natural Hazards and Earth System Sciences, 13*(12), 3493–3501.

Pereira, E., Tassinari, C. C., Rodrigues, J. F., & Van-Dúnem, M. V. (2011). New data on the deposition age of the volcano-sedimentary Chela Group and its Eburnean basement: Implications to post-Eburnean crustal evolution of the SW of Angola. *Comunicações Geológicas, 98*, 29–40.

Prasad, G., Gusain, G. S., Joshi, V., & Ramola, R. C. (2010). Assessment of dose due to exposure to indoor radon and thoron progeny. *Nuclear Technology and Radiation Protection, 25*(3), 198–204.

Preetz, H., Altfelder, S., Hennings, V., Igel, J. (2009). Classification of soil magnetic susceptibility and prediction of metal detector performance: Case study of Angola. In *Detection and sensing of mines, explosive objects, and obscured targets* XIV (Vol. 7303, p. 730313). International Society for Optics and Photonics.

R Core Team. (2021). R: A language and environment for statistical computing. R Foundation for Statistical Computing, Vienna, Austria. http://www.R-project.org/

Ramola, R. C., Prasad, M., Kandari, T., Pant, P., Bossew, P., Mishra, R., & Tokonami, S. (2016). Dose estimation derived from the exposure to radon, thoron and their progeny in the indoor environment. *Scientific Reports, 6*(1), 1–16.

Regenspurg, S., Margot-Roquier, C., Harfouche, M., Froidevaux, P., Steinmann, P., Junier, P., & Bernier-Latmani, R. (2010). Speciation of naturally-accumulated uranium in an organic-rich soil of an alpine region (Switzerland). *Geochimica Et Cosmochimica Acta, 74*(7), 2082–2098.

Revelle, W. (2020). psych: Procedures for personality and psychological research. Evanston: Northwestern University. https://CRAN.R-project.org/package=psych, version 2.0.12.

Ruffell, A. (2016). Do spectral gamma ray data really reflect humid–arid palaeoclimates? A test from Palaeogene Interbasaltic weathered horizons at the Giant's Causeway, N. Ireland. *Proceedings of the Geologists Association, 127*(1), 18–28.

Ruffell, A., & Worden, R. (2000). Palaeoclimate analysis using spectral gamma-ray data from the Aptian (Cretaceous) of southern England and southern France. *Palaeogeography, Palaeoclimatology, Palaeoecology, 155*(3–4), 265–283.

Sainz, C., Quindós, L. S., Fuente, I., Nicolás, J., & Quindós, L. (2007). Analysis of the main factors affecting the evaluation of the radon dose in workplaces: The case of tourist caves. *Journal of Hazardous Materials, 145*(3), 368–371.

Sakoda, A., Ishimori, Y., & Yamaoka, K. (2011). A comprehensive review of radon emanation measurements for mineral, rock, soil, mill tailing and fly ash. *Applied Radiation and Isotopes, 69*(10), 1422–1435.

Salminen, R., Batista, M.J., Bidovec, M., Demetriades, A., De Vivo, B., De Vos, W., Duris,M., Gilucis, A., Gregorauskiene, V., Halamic, J., Heitzmann, P., Lima, A., Jordan, G., Klaver, G., Klein, P., Lis, J., Locutura, J., Marsina, K., Mazreku, A., O'Connor, P.J., Olsson, S., Ottesen,R.T., Petersell, V., Plant, J.A., Reeder, S., Salpeteur, I.,Sandström, H., Siewers, U., Steenfeldt, A., Tarvainen, T. (2005). *FOREGS geochemical atlas of Europe, part 1: Background information, methodology and maps*. Geological Survey of Finland, Otamedia Oy, Espoo, Finland (p. 525).

Salupeto-Dembo, J., Völgyesi, P., Szabó, Z., & Szabó, C. (2018). Contribution of thoron to the inhalation dose in Angolan adobe houses. In Kovács, T., Tóth-Bodrogi, E., & Bátor, G. (Eds). VI. *Terrestrial radiosotopes in environment. International conference on environmental protection*, Vesprém (p. 55).

Salupeto-Dembo, J., Szabó-Krausz, Z., Völgyesi, P., & Szabó, C. (2020). Radon and thoron radiation exposure of the Angolan population living in adobe houses. *Journal of Radioanalytical and Nuclear Chemistry, 325*, 271–282.

Scheib, C., Appleton, J. D., Miles, J. C. H., & Hodgkinson, E. (2013). Geological controls on radon potential in England. *Proceedings of the Geologists' Association, 124*(6), 910–928.

Sêco, S. L., Domingos, F. P., Pereira, A. J. S. C., & Duarte, L. V. (2020). Estimation of the radon production potential in sedimentary rocks: A case study in the Lower and Middle Jurassic of the Lusitanian Basin (Portugal). *Journal of Environmental Radioactivity, 220*, 106272.

Sêco, S. L. R., Pereira, A. J. S. C., Duarte, L. V., & Domingos, F. (2021). Sources of uncertainty in field gamma-ray spectrometry: Implications for exploration in the Lower-Middle Jurassic sedimentary succession of the Lusitanian Basin (Portugal). *Journal of Geochemical Exploration, 227*, 106799. https://doi.org/10.1016/j.gexplo.2021.106799

Shang, B., Chen, B., Gao, Y., Wang, Y., Cui, H., & Li, Z. (2005). Thoron levels in traditional Chinese residential dwellings. *Radiation and Environmental Biophysics, 44*(3), 193–199.

Singh, S., Kumar, M., & Mahajan, R. K. (2005). The study of indoor radon in dwellings of Bathinda district, Punjab, India and its correlation with uranium and radon exhalation rate in soil. *Radiation Measurements, 39*(5), 535–542.

Somogyi, G., Paripas, B., & Varga, Z. (1984). Measurement of radon, radon daughters and thoron concentrations by multi-detector devices. *Nuclear Tracks and Radiation Measurements, 8*(1–4), 423–427.

Sorimachi, A., Tokonami, S., Omori, Y., & Ishikawa, T. (2012). Performance test of passive radon–thoron discriminative detectors on environmental parameters. *Radiation Measurements, 47*(6), 438–442.

Szeiler, G., Somlai, J., Ishikawa, T., Omori, Y., Mishra, R., Sapra, B. K., Mayya, Y. S., Tokonami, S., Cordás, A., & Kovács, T. (2012). Preliminary results from an indoor radon thoron survey in Hungary. *Radiation Protection Dosimetry, 152*(1–3), 243–246.

Tokonami, S. (2010). Why is ^{220}Rn (thoron) measurement important? *Radiation Protection Dosimetry, 141*(4), 335–339.

Tokonami, S., Takahashi, H., Kobayashi, Y., Zhuo, W., & Hulber, E. (2005). Up-to-date radon-thoron discriminative detector for a large scale survey. *Review of Scientific Instruments, 76*(11), 113505.

Torquato, J. R., & Forgaça, A. C. (1981). Correlação entre o Supergrupo Espinhaço no Brasil, o Grupo Chela em Angola e as formações Nosib e Khoabendus da Namíbia. In: Anais do Simpósio sobre o Craton do São Francisco e suas Faixas Marginais, Sociedade Brasileira de Geologia/Coordenação da Produção Mineral, Salvador (pp. 87–98).

Torquato, J., Silva, A., Cordani, U., & Kawashita, K. (1979). Evolução geológica do cinturão móvel do Quipungo. *Academia Brasileira Ciências, 51*(1), 133–144.

UNSCEAR, United Nation Scientific Committee on the Effect of Atomic Radiation. (2000). Annex B: Exposures from Natural Radiation Sources. United Nations (p. 104).

UNSCEAR, United Nations Scientific Committee on the Effects of Atomic Radiation. (2010). Source and effects of ionizing radiation. UNSCEAR 2008, report to the general assembly with scientific annexes (Vol. I, p. 463).

Vaupotič, J., & Kávási, N. (2010). Preliminary study of thoron and radon levels in various indoor environments in Slovenia. *Radiation Protection Dosimetry, 141*(4), 383–385.

Virk, H. S., & Sharma, N. (2000). Indoor radon/thoron survey report from Hamirpur and Una districts, Himachal Pradesh, India. *Applied Radiation and Isotopes, 52*(1), 137–141.

WHO, World Health Organization. (2009). WHO handbook on indoor radon—A public health perspective. WHO Library Cataloguing-in-Publication Data (p. 110).

Zhuo, W., Tokonami, S., Yonehara, H., & Yamada, Y. (2002). A simple passive monitor for integrating measurements of indoor thoron concentrations. *Review of Scientific Instruments*, *73*(8), 2877–2881.

Zunic, Z. S., Stojanovska, Z., Veselinovic, N., Mishra, R., Yarmoshenko, I. V., Sapra, B. K., Ishikawa, T., Omori, Y., Curguz, Z., Bossew, P., Udovocic, V., & Ramola, R. C. (2017). Indoor radon, thoron and their progeny concentrations in high thoron rural Serbia environments. *Radiation Protection Dosimetry, 177*(1–2), 36–39.